Brazilian Journal of Geophysics (2022) 40, 2, 299-310
Brazilian Geophysical Society
ISSN 2764-8044
DOI: 10.22564/brjg.v40i2.2167

# THERMAL STATE OF THE LITHOSPHERE OF PATAGONIA VIA DATA OF THE XENOLITHS

Carlos Henrique Alexandrino, Carlos Alberto Mirez Tarrillo, André Froede Silva, Juliana de Oliveira Batista and Carlos Eduardo Cardoso Nogueira

Universidade Federal dos Vales do Jequitinhonha e Mucuri – UFVJM, Teófilo Otoni, MG, Brazil

*Corresponding author email: carlos.alexandrino@ufvjm.edu.br

**ABSTRACT.** Ultramafic xenoliths and minerals present in intrusive rocks make it possible to infer the temperature and pressure of the upper mantle and lower crust, since they preserve their physical and chemical characteristics while being transported by magmatic processes. Thermal models incorporating thermobarometric data have been developed to estimate the thermal field. Thus, the objective of this work is to use information about mineralogical temperature and pressure equilibrium to estimate lithospheric thermal field in the Patagonian region bounded by latitudes 40º - 52º S and longitudes 67º - 71º W. These coordinates correspond to the Argentine provinces of Río Negro, Chubut and Santa Cruz. Experimental mineral temperature data indicate ranges of 917-1029 ºC in the Chubut province, 877-1253 ºC in the Río Negro region and 728-1196 ºC in the Santa Cruz province. The average heat flux and temperature values at Moho depth are 40 mWm$^{-2}$ and 734 ºC, respectively. Río Negro province has the highest temperature (760 ± 45 ºC) and the lowest thermal thickness value (75 ± 11 km), while Santa Cruz province has the highest heat flux (44 ± 7 mWm$^{-2}$) at Moho depth, which indicates that there are possibly two plumes responsible for the deposition of xenoliths in the region: one in Río Negro province and the other in Santa Cruz.

**Keywords:** heat flow, radiogenic heat production, thermal thickness, coefficient of the variation of thermal conductivity with temperature, geothermobarometry.

## INTRODUCTION

Ultramafic xenoliths (peridotite-pyroxenites) and eclogitic minerals present in intrusive rocks such as kimberlites, lamproites and alkaline basalts are widely used to infer the temperature and pressure of the upper mantle and lower crust (Kukkonen and Peltonen, 1999; Russell and Kopylova, 1999; Russell et al., 2001; Aulbach et al., 2004; Harder and Russell, 2006; Howarth et al., 2014; Dymshits et al., 2020; and Alexandrino et al., 2022). As xenoliths preserve their physical and chemical characteristics while being transported by magmatic processes, we can use this information to estimate the thermal field of the lithosphere using the thermobarometric equilibrium condition of xenoliths. The method was used by Rudnick et al. (1998) in a global study with the purpose of investigating the thermal regime in Archaean terrains. Russell et al. (2001) evaluated radiogenic heat production and basal heat flow in the Slave Craton region of Canada via thermobarometrical xenolith data. A similar method was also used by Dymshits et al. (2020) to estimate the thermal state, thickness and composition of the Siberian Craton. These studies show that the information extracted via equilibrium conditions from samples of xenoliths of man-made origin constitutes an efficient way to infer geothermal parameters of the lithosphere, especially in the upper mantle and lower crust.

In this context, the region of Patagonia in Argentina provides an opportunity to infer geothermal parameters. at Moho's depth being covered by geologically recent basaltic volcanism it provides samples of ultramafic xenoliths directly from the upper mantle from data compiled in works published in the past two decades (Mallmann, 2004; Bjerg et al., 2005; Ntaflos et al., 2007; Rieck Jr. et al., 2007; Schilling et al.. 2017).

Therefore, the objective of our study to evaluate the usefulness to estimate the thermal state of the crustal lithosphere and mantle based on the information about mineralogical temperature and pressure equilibrium.

## GEOLOGIC SETTING

The study area is located between the latitudes 40º and 52º S and the longitudes 67º and 71º W. These coordinates delimit the Patagonian region, the focus of this work which also includes the southern stretch of the Andes, as described in Figure 1, where the main pre-Jurassic tectonic elements are the Northern Patagonian and the Deseado Massifs (Caminos et al., 1999; Giacosa et al., 2012).

In these regions there is a Jurassic rhyolitic volcanic rock domain which forms one of the largest siliceous provinces in the world (Pankhurst et al., 1998).

The siliceous volcanic field of Patagonia extends from the Atlantic coast to the Chilean Andean region. The Eastern Patagonia is geologically divided into stable areas, in which the volcanic rocks are now exposed in the Northern and Deseado Patagonian massifs and the intermediate areas are covered by the Cretaceous and Tertiary sedimentary rock; NGHBVFDs of the San Jorge and Magellan Basins (Pankhurst et al., 1998; Caminos et al., 1999).

The most important geological units in the region are the Choiyoi complex (Triassic-Jurassic), the Chon Aike complex (Jurassic-Cretaceous) and the plutonic rocks (Permo-Triassic) (Caminos et al., 1999; Giacosa et al., 2012).

The basement rocks occupy a larger area in the Northern Patagonian Massif. The main types of rocks which occur on the western edge of the massif in Paleozoic granite intrusions are shales and gneiss. Carboniferous and Permian gneisses occur in the southwestern part of the massif (Pankhurst et al., 1998; 2006; Caminos et al., 1999).

In the Deseado massif, it occurs a series of small outcrops that reveal sequences of micaceous materials and amphibolitic shales, possibly of pre-Cambrian or late Cambrian age. Permo-Triassic conglomerates fill small basins and represent the oldest evidence of an extensional regime that became more pronounced during the Triassic period with the regional formation of the NNW-SSE trend graben throughout Patagonia (Pankhurst et al., 1998).

## MATERIALS AND METHODS

Outcrops of xenoliths in the form of alkaline basaltic lavas occur in various areas of Patagonia. Samples from these outcrops were collected by Ntaflos et al. (2007) in the region limited by latitudes 40º and 52º S and longitudes 67º and 71º W, occurring in the provinces of Río Negro, Chubut and Santa Cruz.

Figure 2 shows the occurrences of xenoliths in the provinces of Río Negro, Chubut and Santa Cruz, Argentina.

Patagonian xenolith samples include harzburgite spinel, harzburgite garnet, lherzolite spinel, websterite spinel and small quantities of wehrlite dunites and pyroxenites in sizes ranging from 1 to 20 cm (Mallmann, 2004; Bjerg et al., 2005; Ntaflos et al., 2007; Rieck Jr. et al., 2007; Schilling et al., 2017).

Tables 1, 2 and 3 present the pressure and temperature information, as well as the types of dominant minerals present in xenolith samples in the provinces of Río Negro, Chubut, and Santa Cruz, compiled from various works, as described in the references. Details on the geothermometers and geobarometers used to estimate the pressure and temperature of equilibrium can be consulted in the references from which the information was compiled.

## MODEL DESCRIPTION

As the main mode of heat transfer in the lithosphere is conduction, we can develop a model to estimate the thermal field of the lithosphere from the following parameters: temperature, heat flow, radiogenic heat production and thermal conductivity.

The model proposed in this work is composed of two layers, as described in Figure 3. This analysis is similar to that proposed by Russell and Kopylova (1999); Lewis et al. (2003); Harder and Russell, (2006); Greenfild et al. (2013); and Alexandrino et al. (2022).

Layer (1) represents the crust with the top on the Earth's surface, where $\mathbf{Z}_0$=0, and the base on the top mantle at the $\mathbf{Z}_M$ position. In this layer the radiogenic heat production $\mathbf{A}_0$ and the thermal conductivity $\boldsymbol{\lambda}_0$ are constant; $\mathbf{T}_0$ represents temperature and $\mathbf{q}_0$ the heat flow, both on the surface.

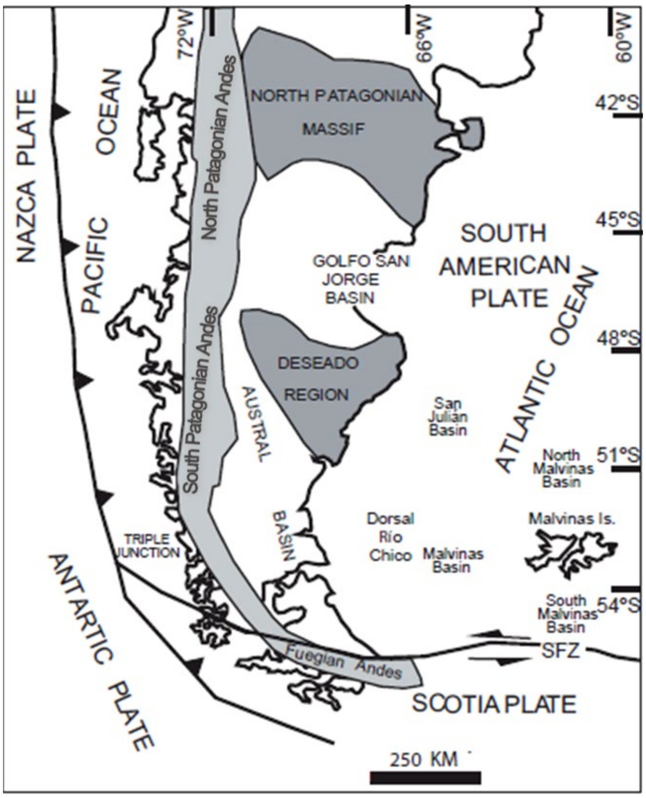


Figure 1: Major geological provinces of Patagonia (Giacosa et al., 2012).

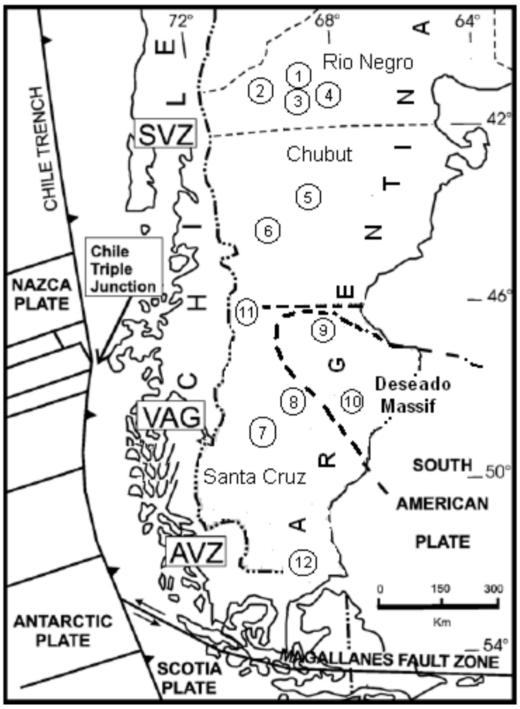


Figure 2: Location of mantle xenoliths in Río Negro, Chubut and Santa Cruz provinces (modified from Ntaflos et al., 2007). The abbreviations used are: SVZ - Southern Volcanic Zone; VGZ - Volcanic Gap Zone; AVZ - Austral Volcanic Zone. The numbers correspond to the following localities: 1- Estancia Alvarez; 2- Cerro de Monjon; 3- Prahuaniyeu; 4- Laguna Fria; 5- Paso de Indios; 6- Cerro de los Chenques; 7- Tres Lagos; 8- Gobernador Gregores; 9- Cerro Clark; 10- Auvernia; 11- Coyhaique; and 12- Pali Aike.

Table 1: Pressure and Temperature (P-T) data on mantle xenoliths in the Chubut Province.

| P (kb) | T (ºC) | Description | Reference |
|---|---|---|---|
| 16 | 917 | Lherzolite | Bjerg et al. (2005) |
| 16 | 917 | Lherzolite | Rieck Jr. et al. (2007) |
| 16 | 899 | Lherzolite | Rieck Jr. et al. (2007) |
| 16 | 928 | Harzburgite | Rieck Jr. et al. (2007) |
| 16 | 928 | Lherzolite | Rieck Jr. et al. (2007) |
| 16 | 927 | Harzburgite | Rieck Jr. et al. (2007) |
| 17 | 949 | Olivine Websterite | Rieck Jr. et al. (2007) |
| 18 | 1005 | Harzburgite | Rieck Jr. et al. (2007) |
| 19 | 1029 | Harzburgite | Rieck Jr. et al. (2007) |
| 19 | 1029 | Harzburgite | Rieck Jr. et al. (2007) |

Table 2: Pressure and Temperature (P-T) data on mantle xenoliths in the Río de Negro Province.

| P (kb) | T (ºC) | Description | Reference |
|---|---|---|---|
| 11 | 877 | Harzburgite | Mallmann (2004) |
| 14 | 914 | Harzburgite | Mallmann (2004) |
| 14 | 936 | Lherzolite | Mallmann (2004) |
| 15 | 942 | Lherzolite | Mallmann (2004) |
| 16 | 993 | Harzburgite | Mallmann (2004) |
| 19 | 1079 | Harzburgite | Mallmann (2004) |
| 17 | 1122 | Spinel Harzburgite | Bjerg et al. (2005) |
| 20 | 1180 | Spinel Harzburgite | Bjerg et al. (2005) |
| 23 | 1200 | Garnet Lherzolite | Bjerg et al. (2005) |
| 24 | 1253 | Spinel Harzburgite | Bjerg et al. (2005) |

Table 3: Pressure and Temperature (P-T) data on mantle xenoliths in the Santa Cruz Province.

| P (kb) | T (ºC) | Description | Reference |
|---|---|---|---|
| 10 | 728 | Spinel Peridotites | Ntaflos et al. (2007) |
| 12 | 830 | Spinel Lherzolite | Bjerg et al. (2005) |
| 13 | 850 | Lherzolite | Schilling et al. (2017) |
| 14 | 884 | Spinel Peridotites | Ntaflos et al. (2007) |
| 15 | 968 | Harzburgite | Schilling et al. (2017) |
| 16 | 1021 | Lherzolite | Schilling et al. (2017) |
| 17 | 1040 | Spinel Peridotites | Ntaflos et al. (2007) |
| 16 | 1055 | Spinel Harzburgite | Bjerg et al. (2005) |
| 16 | 1057 | Lherzolite | Schilling et al. (2017) |
| 16 | 1064 | Harzburgite | Schilling et al. (2017) |
| 22 | 1196 | Spinel Lherzolite | Bjerg et al. (2005) |
| 24 | 1260 | Garnet Harzburgite | Bjerg et al. (2005) |

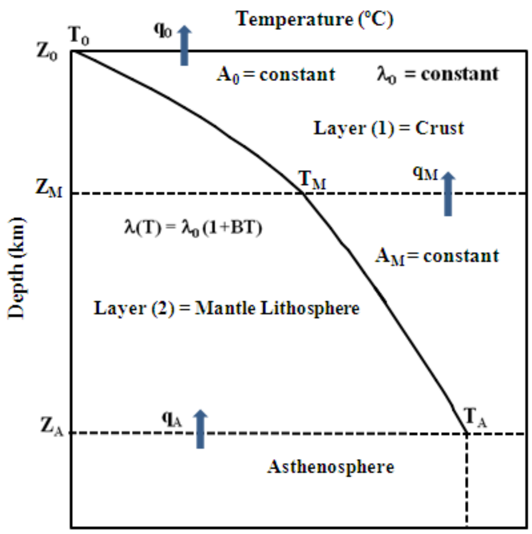


Figure 3: Schematic representation of the model for conductive heat transfer in the crust and mantle lithosphere.

Layer (2) represents the lithospheric mantle. The top of this region is at the $\mathbf{Z_M}$ position and the base at the $\mathbf{Z_A}$ position. $\mathbf{Z_M}$ is the Moho's depth; therefore, it also represents the crustal thickness. The radiogenic heat production $\mathbf{A_M}$ in layer (2) is assumed to be constant, but the thermal conductivity $\boldsymbol{\lambda}$(T) is a function of temperature, and **B** is the coefficient of the variation of thermal conductivity with temperature. $\mathbf{T_M}$ and $\mathbf{q_M}$ are respectively the temperature and the heat flow at Moho's depth.

The $\mathbf{Z_A}$ position physically represents the thickness of the thermal lithosphere, which is the region of the lithosphere where by definition the main mode of heat transfer is conduction. In this position, temperature $\mathbf{T_A}$ has a value of approximately 1300ºC and $\mathbf{q_A}$ represents the heat flow from the asthenosphere.

Based on the schematic representation presented in Figure 3, we can formulate the temperature distribution in the lithosphere for layers (1) and (2) from the one-dimensional equation of heat in permanent regime. In these conditions, equation (1a) can be considered as representative of the thermal field for layer (1). Equations (1b) and (1c) are the contour conditions. In this layer the thermal conductivity and the radiogenic heat production are assumed to be constant.

$$\frac{d^2T_1}{dZ^2} = -\frac{A_0}{\lambda_0} \qquad Z_0 < Z < Z_M \qquad (1a)$$

$$T_1(Z = Z_0) = T_0 \qquad (1b)$$

$$T_1(Z = Z_M) = T_M \qquad (1c)$$

where $T_1$ represents temperature, and the other variables are those described and informed in Figure 3. The solution to the boundary value problem described by equations (1a), (1b) and (1c) is shown in equation (2).

$$T_1(Z) = -\frac{A_0}{2\lambda_0}Z^2 + \left[\left(\frac{T_M - T_0}{Z_M}\right) + \frac{A_0}{2\lambda_0}Z_M\right]Z + T_0 \qquad (2)$$

Equation (2) represents the temperature distribution for layer (1). Equation (3a) shows the formulation for layer (2). Equations (3b) and (3c) are the boundary conditions and equation (3d) shows the variation of thermal conductivity with temperature. The radiogenic heat production in this layer is assumed to be constant.

$$\frac{d}{dZ}\left[\lambda(T_2)\frac{dT_2}{dZ}\right] = -A_M \qquad Z_M < Z < Z_A \qquad (3a)$$

$$T_2(Z = Z_M) = T_M \qquad (3b)$$

$$\lambda(T_2)\frac{dT_2}{dZ} = q_M \qquad (3c)$$

$$\lambda(T_2) = \lambda_0(1 + BT_2) \qquad (3d)$$

where $T_2$ represents temperature, and the other variables are those described and informed in Figure 3. The solution to the boundary value problem described by equations (3a), (3b), (3c) and (3d) is presented in equation (4).

$$T_2(Z) = \frac{q_M}{\lambda_0}(Z - Z_M) - \frac{A_M}{2\lambda_0}(Z - Z_M)^2 - \frac{B}{2}[T_2(Z) - T_M]^2 + T_M \quad (4)$$

Equation (4) represents the temperature distribution for layer (2). The solution of equation (1) was obtained by applying conventional methods for solving differential equations with these characteristics. The solution of equation (3a) was obtained by applying Kirchhoff Transform to remove nonlinearity and consequently transform the nonlinear problem into a linear one (for details, see Özisik and Hahn, 2012). This technique was used by Dipple and Kopylova (2000) and Russell et al. (2001) to determine the production and flow of heat in the region of the Slave Craton, Canada. Alexandrino and Hamza (2008) used this technique to estimate the thermal field of the Brazilian geological province of São Francisco.

## METHODOLOGY TO ESTIMATE THE GEOTHERMAL PARAMETERS

To use the model proposed in this work, it is necessary to know some initial information which is in Table 4. $T_0$ is the average annual surface temperature of the study area. The thermal conductivity $\lambda_0$ and the density ρ have similar values to those used by Russell and Kopylova (1999), Lewis et al. (2003), Harder and Russell (2006), and Greenfield et al. (2013). According to Chulick et al. (2013) and Lloyd et al. (2010), the crustal thickness $Z_M$ in the Patagonia region is between 28 and 32 km.

Results from numerical simulations indicate that small variations in the value of $Z_M$ do not significantly affect estimates of lithospheric thicknesses. Thus, we assumed the average value of 30 km as the characteristic of the crustal thickness of the region.

Table 4: Physical parameters used in the model.

| Property | Lithospheric Layers | |
|---|---|---|
| | Crust | Mantle |
| $T_0$ (ºC) | 10 | --- |
| $Z_M$ (km) | 30 | --- |
| $\lambda_0$ (W m$^{-1}$ ºC$^{-1}$) | 2.5 | 3.0 |
| ρ (kg m$^{-3}$) | 2700 | 3300 |

Below we describe the sequential process to estimate the geothermal parameters of interest.

### Geothermal parameters at Moho depth

To estimate the geothermal parameters at the depth of Moho such as temperature $T_M$, heat flow $q_M$, radiogenic heat production $A_M$ and the coefficient of the variation of thermal conductivity with temperature B at the depth of Moho, we used the pressure and temperature balance data described in Tables 1, 2 and 3; the physical parameters described in Table 4; and equation (4) to form a system of equations.

The system of equations formed from temperature and pressure balance data allows us to estimate $T_M$, $q_M$, $A_M$ and B at Moho depth using appropriate numerical methods. In this work we used the RNLIN routine available in IMSL. The RNLIN routine uses a modified Levenberg-Marquardt method.

### Radiogenic heat production in the surface $A_0$

To estimate the heat production at the surface, we derived equation (2), thus obtaining equation (5).

$$\frac{dT_1}{dZ}(Z) = -\frac{A_0}{\lambda_0}Z + \left[\left(\frac{T_M - T_0}{Z_M}\right) + \frac{A_0}{2\lambda_0}Z_M\right] \quad (5)$$

We evaluated equation (5) at the $Z=Z_M$ position and multiplied the resulting equation by $\lambda_0$. Following this procedure, we arrived at equation (6) and thus we could estimate $A_0$.

$$A_0 = \frac{2}{Z_M}\left[\lambda_0\left(\frac{T_M - T_0}{Z_M}\right) - q_M\right] \quad (6)$$

### Geothermal heat flow in the surface $q_0$

To estimate the value of the heat flow at the surface, we multiplied equation (5) by $\lambda_0$ evaluated at position $Z=Z_0=0$.

$$q_0 = \lambda_0\left(\frac{T_M - T_0}{Z_M}\right) + \frac{A_0}{2}Z_M \quad (7)$$

## RESULTS AND DISCUSSION

Tables 5, 6 and 7 present the results of the geothermal parameter estimates for the provinces of Río Negro, Chubut and Santa Cruz. The values of the coefficient of the variation of thermal conductivity with temperature and radiogenic heat production in all provinces are compatible with those expected for these parameters (Jaupart and Mareschal, 1999; Kukkonen and Peltonen, 1999; Russell et al., 2001; Artemieva and Mooney, 2001; Dymshits et al., 2020).

Table 5: Summary of model results for geothermal parameters of the Río Negro province.

| **Río Negro province model parameters** | | | | |
|---|---|---|---|---|
| **Property** | **Estimate** | | | |
| | **Lower** | **Upper** | **Best** | **±** |
| $T_M$ (ºC) | 712 | 788 | 750 | 38 |
| $q_0$ ($mWm^{-2}$) | 73 | 84 | 79 | 5 |
| $q_M$ ($mWm^{-2}$) | 39 | 50 | 44 | 6 |
| $A_0$ ($\mu Wm^{-3}$) | 1.0 | 1.4 | 1.2 | 0.2 |
| $A_M$ ($\mu Wm^{-3}$) | $2.5x10^{-2}$ | $3.2x10^{-2}$ | $2.8x10^{-2}$ | $3.5x10^{-3}$ |
| B ($W\ m^{-1}\ ºC^{-2}$) | $1.3x10^{-4}$ | $1.7x10^{-4}$ | $1.5x10^{-4}$ | $1.9x10^{-5}$ |
| $Z_A$ (km) | 65 | 86 | 75 | 11 |

Table 6: Summary of model results for geothermal parameters of the Chubut province.

| **Chubut province model parameters** | | | | |
|---|---|---|---|---|
| **Property** | **Estimate** | | | |
| | **Lower** | **Upper** | **Best** | **±** |
| $T_M$ (ºC) | 659 | 730 | 693 | 36 |
| $q_0$ ($mWm^{-2}$) | 73 | 83 | 78 | 5 |
| $q_M$ ($mWm^{-2}$) | 31 | 41 | 36 | 5 |
| $A_0$ ($\mu Wm^{-3}$) | 1.2 | 1.6 | 1.4 | 0.2 |
| $A_M$ ($\mu Wm^{-3}$) | $1.0x10^{-2}$ | $1.4x10^{-2}$ | $1.2x10^{-2}$ | $2.0x10^{-3}$ |
| B ($W\ m^{-1}\ ºC^{-2}$) | $1.2x10^{-4}$ | $1.6x10^{-4}$ | $1.4x10^{-4}$ | $2.0x10^{-5}$ |
| $Z_A$ (km) | 76 | 102 | 87 | 13 |

Table 7: Summary of model results for geothermal parameters of the Santa Cruz province.

| **Santa Cruz province model parameters** | | | | |
|---|---|---|---|---|
| **Property** | **Estimate** | | | |
| | **Lower** | **Upper** | **Best** | **±** |
| $T_M$ (ºC) | 715 | 804 | 760 | 45 |
| $q_0$ ($mWm^{-2}$) | 78 | 91 | 85 | 7 |
| $q_M$ ($mWm^{-2}$) | 34 | 47 | 40 | 7 |
| $A_0$ ($\mu Wm^{-3}$) | 1.2 | 1.8 | 1.5 | 0.3 |
| $A_M$ ($\mu Wm^{-3}$) | $1.9x10^{-2}$ | $2.7x10^{-2}$ | $2.5x10^{-2}$ | $3.8x10^{-3}$ |
| B ($W\ m^{-1}\ ºC^{-2}$) | $2.7x10^{-4}$ | $3.7x10^{-4}$ | $3.5x10^{-4}$ | $5.3x10^{-5}$ |
| $Z_A$ (km) | 69 | 98 | 82 | 15 |

In the province Río Negro, it can be seen in Table 5 that the heat flow varies from 73 to 84 $mWm^{-2}$ and the radiogenic heat production from 1.0 to 1.3 $\mu Wm^{-3}$ in the surface. At Moho's depth, the temperature and the heat flow have average values of 750 °C and 44 $mWm^{-2}$, respectively, and the thermal thickness of this province has a value of 75 km, which is the lowest thermal thickness estimated in this work.

Table 6 shows the geothermal parameter estimates for the Chubut province. In this province the estimated thermal thickness is between 76 and 102 km. The average values of heat flow and radiogenic heat production at the surface are respectively 78 $mWm^{-2}$ and 1.4 $\mu Wm^{-3}$. At the depth of Moho, 36 $mWm^{-2}$ is the value of the heat flow and 693 °C the temperature. These are the lowest values of geothermal parameters at Moho's depth among the three provinces.

For the province of Santa Cruz, the parameter values are shown in Table 7. In this province the heat flow varies from 78 to 91 $mWm^{-2}$ and the radiogenic heat production from 1.2 to 1.8 $\mu Wm^{-3}$ in the surface. These are the highest values when compared to the other provinces. At Moho's depth, the parameters vary as follows: temperature between 715 and 804 °C and heat flow from 34 to 47 $mWm^{-2}$. The average thermal thickness estimated for the province was 82 km.

The uncertainties in the estimates of the magnitudes listed in Tables 5, 6 and 7 come from a number of sources, including uncertainties of $Z_M$ crustal thickness, pressure, temperature and composition of the xenolith samples, listed in Tables 1, 2 and 3, and the value of the thermal conductivity $\lambda_0$.

To minimize these problems, a model of radiogenic heat production and constant thermal conductivity in the crust (layer 1 of Figure 3), and constant heat production in the lithospheric mantle (layer 2 of Figure 3) was chosen to reduce the number of variables in the model and consequently obtain more robust results.

Because, at Moho's depth, the value of temperature $T_M$ is associated with crustal thickness and the value of heat flow $q_M$ with the value of thermal conductivity, all cases were simulated considering $Z_M$ = 30 km and $\lambda_0$ = 3.0 W $m^{-1}$ $°C^{-1}$ in the lithospheric mantle (layer 2, Figure 3). Therefore, the quantities $T_M$ and $q_M$ (equation 4) are influenced only by the production of the $A_M$ radiogenic heat and the coefficient of the variation of thermal conductivity B.

In relation to the production of radiogenic heat in the mantle, the global data indicate that the values of this parameter are in the range of $10^{-6} < A_M < 0.06$ $\mu Wm^{-3}$. This represents a variation of ± 5.0 °C in the temperature value $T_M$ and ± 2.0 $Wm^{-2}$ in the value of the heat flow $q_M$.

According to Kukknen and Jõeleht (1995), Seipold (1998), Jaupart and Mareschal (1999), Artemieva and Mooney (2001), and Seipold (2001), for parameter B, the typical values in the lithospheric mantle are between $1x10^{-4} < B < 5x10^{-4}$ $Wm^{-1}°C^{-2}$, which causes a variation of ± 10 °C in the $T_M$ temperature value.  in the flow of heat $q_M$ this variation is around ± 4.0 $mWm^{-2}$.

The other constraint used to solve equation (4) was to establish a difference between the observed temperature $T_{OBS}$ and the $T_{MODEL}$ below or equal to 20°C.

This value was chosen due to the uncertainty in the thermobarometry calibration estimated at ± 20 °C and ± 0.3 GPa for the geothermometer proposed by Brey and Köhler, 1990. Figures 4, 5 and 6 show the results of the temperature distribution for the provinces Río Negro, Chubut and Santa Cruz. In the figures we can observe the maximum and minimum values of the modelled temperature profiles as well as the observed data.

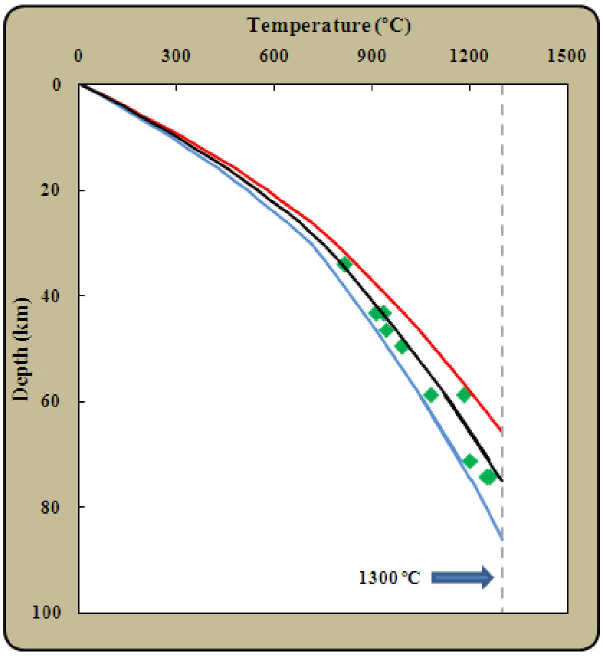


Figure 4: Temperature distribution of Río Negro province. The red line represents the upper limits; the blue line, the lower limit; and the black one, the best fit. The limits were established with 95% confidence. The gray dotted line represents the isotherm of 1300 °C and the green dots are the observed data.

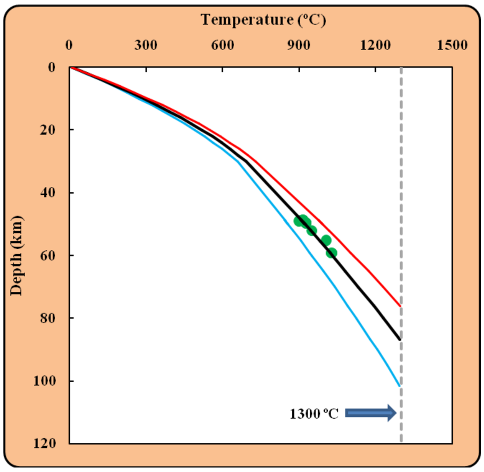


Figure 5: Temperature distribution of Chubut province. The red line represents the upper limits, the blue line, the lower limit, and the black one, the best fit. The limits were established with 95% confidence. The gray dotted line represents the isotherm of 1350 °C and the green dots are the observed data.

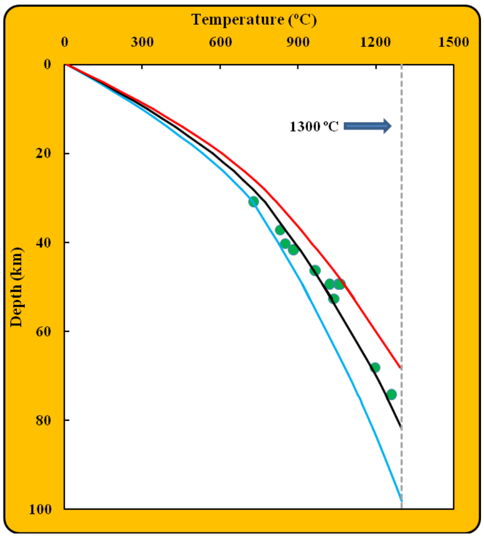


Figure 6: Temperature distribution of Santa Cruz province. The red line represents the upper limits, the blue line, the lower limit, and the black one, the best fit. The limits were established with 95% confidence. The gray dotted line represents the isotherm of 1350 °C and the green dots are the observed data.

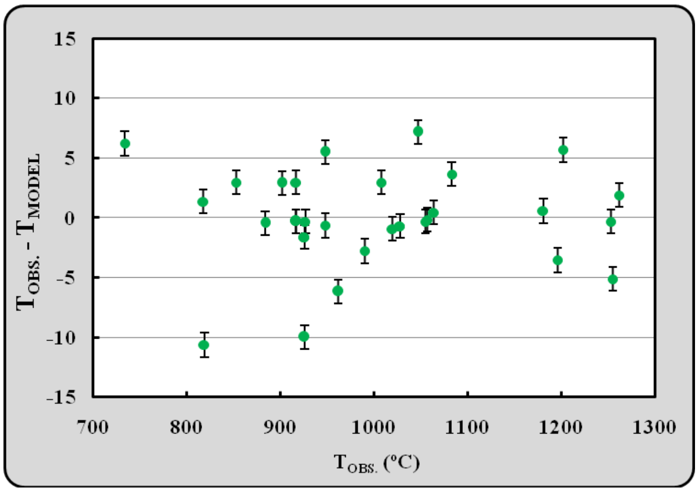


Figure 7: Residue (difference between observed and modelled temperature) versus observed temperature. The residues are below 15 °C.

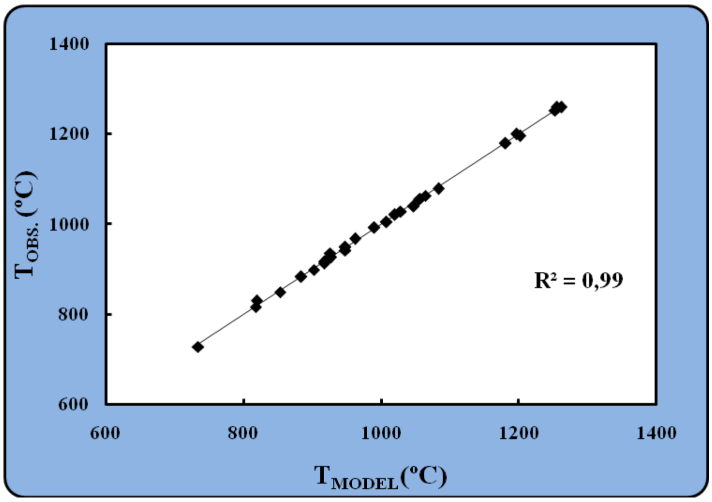


Figure 8: Relationship between observed and modelled data. The value of R2 shows strong correlation between the observed and modelled temperatures.

Figure 7 shows that the strategy of fixing $Z_M$ and $\lambda_0$ should be used to refine the values of $A_M$ and B within the range of expected values for these quantities. It was possible to estimate the variables $T_M$, $A_M$, $q_M$, and B in equation (4) in order to obtain the difference between $T_{OBS}$ and $T_{MODEL}$ within the range of uncertainties of the geothermobarometer.

Imposing these restrictions, we obtain a good quality of the adjustment, as can be verified by the analysis of Figure 8, where we can observe that the correlation coefficient $R^2 > 0.99$ confirms a strong correlation between the observed data and those predicted by the model.

## CONCLUSIONS

From the mineralogical equilibrium data of temperature and pressure, considering only the average values, we can infer the geothermal parameters for the lithosphere in the Patagonian region bounded by latitudes 40° - 52° S and longitudes 67° - 71° W. These coordinates correspond to the Argentine provinces of Río Negro, Chubut and Santa Cruz.

Therefore, the values of the geothermal parameters near the surface are 81 $mWm^{-2}$ and 1.4 $\mu Wm^{-3}$ for the heat flow and radiogenic heat production, respectively; at Moho depth, the values are 40 $mWm^{-2}$ for heat flow, $2x10^{-2}$ $\mu Wm^{-3}$ for radiogenic heat production and 734 °C for temperature. It was estimated 81 km for the thermal thickness and $2x10^{-4}$ W $m^{-1}$ $°C^{-2}$ for the coefficient of the variation of thermal conductivity with temperature.

The value of the heat flow at the surface is like those estimated by Cardoso et al. (2010), Ávila and Dávila (2018) and Vieira and Hamza (2019). The radiogenic heat production and the parameter of the variation of thermal conductivity at Moho's depth are within the range of expected values, so we can consider that the model presents coherent results, which may better show the applications of the model when more accurate data are available.

Santa Cruz province has the highest heat flow at the surface and the highest temperature value at Moho depth. Río Negro province has the lowest thermal thickness value and the highest heat flow at Moho depth, indicating that there are possibly two plume heads responsible for xenolith deposition in the region: one in Río Negro province and the other in Santa Cruz.

## REFERENCES

Alexandrino, C. H., and V. M. Hamza, 2008, Estimates of heat flow and heat production and a thermal model of the São Francisco Craton: International Journal of Earth Sciences, **97**, 2, 289–306, doi: 10.1007/s00531-007-0291-y.

Alexandrino, C. H., C. A. M. Tarrillo, A. F. Silva, J. O. Batista, C. E. C. Nogueira, 2022, Thermal state of the lithosphere in Eastern Paraguay and in Andean Domain (South American Platform): International Journal of Terrestrial Heat Flow and Applied Geothermics, **5**, 55–61, doi: 10.31214/ijthfa.v5i1.87.

Artemieva, I.M., and W.D. Mooney, 2001, Thermal thickness and evolution of Precambrian lithosphere: A global study: Journal of Geophysical Research: Solid Earth, **106**, B8, 16387–16414, doi: 10.1029/2000JB900439.

Aulbach, S., W. L. Griffin, S. Y. O'Reilly, and T. E. McCandless, 2004, Genesis and evolution of the lithospheric mantle beneath the Buffalo Head Terrane, Alberta (Canada): Lithos, **77**, 1–4, 413–451, doi: 10.1016/j.lithos.2004.04.020.

Ávila, P., and F. M. Dávila, 2018, Heat flow and lithospheric thickness analysis in the Patagonian asthenospheric windows, southern South America: Tectonophysics, **747–748**, 99–107, doi: 10.1016/j.tecto.2018.10.006.

Bjerg, E.A., T. Ntaflos, G. Kurat, G. Dobosi, and C. H. Labudía, 2005, The upper mantle beneath Patagonia, Argentina, documented by xenoliths from alkali basalts: Journal of South American Earth Sciences, **18**, 2, 125–142, doi: 10.1016/j.jsames.2004.09.002.

Brey, G.P. and T. Köhler, 1990, Geothermobarometry in Four-Phase Lherzolites II. New thermobarometers, and practical assessment of existing thermobarometers: Journal of Petrology, **31**, 6, 1353–1378, doi: 10.1093/petrology/31.6.1353.

Caminos, R., J. L. Panza, M. P. Etcheverría, N. E. Pezzutti, and D. C. Rastelli, 1999, Geología Argentina. Instituto de Geología y Recursos Minerales: Servicio Geológico Minero Argentino, Buenos Aires, Annals, **29**, 796 p.

Cardoso, R. R., V. M. Hamza, and C. Alfaro, 2010, Geothermal Resource Base for South America: A Continental Perspective: World Geothermal Congress 2010, Bali, Indonesia, Proceedings World Geothermal Congress, April 2010, p. 25–29.

Chulick, G. S., S. Detweiler and W. D. Mooney, 2013, Seismic structure of the crust and uppermost mantle of South America and surrounding oceanic basins: Journal of South American Earth Sciences, **42**, 260–276, doi: 10.1016/j.jsames.2012.06.002.

Dymshits, A. M., I. S. Sharygin, V. G. Malkovets, I. V. Yakovlev, A. A. Gibsher, T. A. Alifirova, S. S. Vorobei, S. V. Potapov, and V. K. Garanin, 2020, Thermal state, thickness, and composition of the lithospheric mantle beneath the Upper Muna kimberlite field (Siberian Craton) constrained by clinopyroxene xenocrysts and comparison with Daldyn and Mirny fields: Minerals, **10**, 549, doi: 10.3390/min10060549.

Giacosa, R., D. Fracchia, and N. Heredia, 2012, Structure of the Southern Patagonian Andes at 49°′S: Geologica Acta, **10**, 3, 265–282.

Greenfield, A. M. R., E. D. Ghent, and J. K. Russell, 2013, Geothermobarometry of spinel peridotites from southern British Columbia: implications for the thermal conditions in the upper mantle: Canadian Journal of Earth Sciences, **50**, 10, 1019–1032, doi: 10.1139/cjes-2013-0037.

Harder, M. and J.K. Russell, 2006, Thermal state of the upper mantle beneath the Northern Cordilleran Volcanic Province (NCVP), British Columbia, Canada: Lithos, **87**, 1–2, 1–22, doi: 10.1016/j.lithos.2005.05.002.

Jaupart, C. and J.C. Mareschal, 1999, The thermal structure and thickness of continental roots: Lithos, **48**, 93–114, doi: 10.1016/S0024-4937(99)00023-7.

Kukkonen, I. T. and A. Jõeleht, 1995, Geothermal modeling of the lithosphere in the central Baltic Shield and its southern slope: Tectonophysics, **255**, 25–45, doi: 10.1016/0040-1951(95)00131-X.

Kukkonen, I. T., and P. Peltonen, 1999, Xenolith-controlled geotherm for the central Fennoscandian Shield: implications for lithosphere-asthenosphere relations: Tectonophysics, **304**, 301–315, doi: 10.1016/S0040-1951(99)00031-1.

Lewis, T. J., R. D. Hyndman, and P. Flück, 2003, Heat flow, heat generation, and crustal temperatures in the northern Canadian Cordillera: Thermal control of tectonics: J. Geophys. Res.: Solid Earth, **108**, B6, 2316, doi: 10.1029/2002JB002090.

Lloyd, S., S. van der Lee, G. S. França, M. Assumpção, and M. Feng, 2010, Moho map of South America from receiver functions and surface waves: J. Geophys. Res., **115**, B11315, doi: 10.1029/2009JB006829.

Mallmann, G., 2004, Processos e componentes mantélicas no Norte da Patagônia (Argentina) e relações com a subducção Andina: evidências petrográficas, geoquímicas e isotópicas em xenólitos ultramáficos mantélicos: M.S. dissertation, Instituto de Geociências, Universidade Federal do Rio Grande do Sul, Porto Alegre, Brazil. http://hdl.handle.net/10183/3909.

Ntaflos, T., E. A. Bjerg, C. H. Labudia, and G. Kurat, 2007, Depleted lithosphere from the mantle wedge beneath Tres Lagos, southern Patagonia, Argentina: Lithos, **94**, 1–4, 46–65, doi: 10.1016/j.lithos.2006.06.011.

Özisik, M. N. and D. W. Hahn, 2012, Heat conduction: 3rd ed., New York. John Wiley & Sons. 718 pp.

Pankhurst, R. J., P. T. Leat, P. Sruoga, C. W. Rapela, M. Márquez, B. C. Storey, and T. R. Riley, 1998, The Chon Aike province of Patagonia and related rocks in West Antarctica: A silicic large igneous province: Journal of Volcanology and Geothermal Research, **81**, 1–2, 113–136, ISSN 0377-0273, doi: 10.1016/S0377-0273(97)00070-X.

Pankhurst, R. J., C. W. Rapela, C. M. Fanning, and M. Márquez, 2006, Gondwanide continental collision and the origin of Patagonia: Earth-Science Reviews, **76**, 3–4, 235–257, doi: 10.1016/j.earscirev.2006.02.001.

Rieck Jr., N., R. V. Conceição, E. Koester, and C. Dantas, 2007, O manto litosférico continental na região do Cerro de Los Chenques, Argentina: evidências de heterogeneidade e metassomatismo: Geologia USP, Série Científica, **7**, 1, 1–17, doi: 10.5327/Z1519-874x2007000100001.

Rudnick, R. L., W. F. McDonough, and R. J. O'Connell, 1998, Thermal structure, thickness and composition of continental lithosphere: Chemical Geology, **145**, 395–411, doi: 10.1016/S0009-2541(97)00151-4.

Russell, J. K. and M. G. Kopylova, 1999. A steady state conductive geotherm for the North central Slave, Canada: Inversion of petrological data from the Jericho kimberlite pipe: Journal of Geophysical Research, **104**, B4, 7089–7101.

Russell, J. K., G. M. Dipple, and M. G. Kopylova, 2001, Heat production and heat flow in the mantle lithosphere to the Slave craton, Canada: Physics of the Earth and Planetary Interiors, **123**, 1, 27–44, doi: 10.1016/S0031-9201(00)00201-6.

Schilling, M. E., R. W. Carlson, A. Tassara, R. V. Conceição, G. W. Bertotto, M. Vásquez, D. Muñoz, T. Jalowitzki, F. Gervasoni, and D. Morata, 2017, The origin of Patagonia revealed by Re-Os systematics of mantle xenoliths. Precambrian Research, **294**, 15–32, doi: 10.1016/j.precamres.2017.03.008.

Seipold, U., 1998, Temperature dependence of thermal transport properties of crystalline rocks — a general law: Tectonophysics, **291**, 1–4, 161–171, doi: 10.1016/S0040-1951(98)00037-7.

Seipold, U. 2001, Der Wärmetransport in kristallinen Gesteinen unter den Bedingungen der kontinentalen Kruste: Scientific Technical Report STR01/13, GeoForschungs-Zentrum Potsdam, Germany. 142 pp.

Vieira, P. F. and V. M. Hamza, 2019, Assessment of Geothermal Resources of South America – A New Look: International Journal of Terrestrial Heat Flow and Applied Geothermics, **2**, 1, 46–57, doi: 10.31214/ijthfa.v2i1.32.

**Alexandrino, C.H.:** bibliographic review, development of computational model, figures and tables, text writing, reference formatting; **Tarrillo, C.A.M.:** bibliographic review, development of computational model, figures and tables, text writing; **Silva, A.F.:** bibliographic review, development of computational model, figures and tables; **Batista, J.O.:** bibliographic review, development of computational model, figures and tables; **Nogueira, C.E.C.:** bibliographic review, development of computational model, figures and tables.

Received on December 31, 2021 / Accepted on April 19, 2022